Published in final edited form as:
Biomaterials. 2012 April ; 33(11): 3071–3082. doi:10.1016/j.biomaterials.2011.12.030.

Multifunctional unimolecular micelles for cancer-targeted drug delivery and positron emission tomography imaging☆

Yuling Xiao[a,1], **Hao Hong**[b,1], **Alireza Javadi**[a], **Jonathan W. Engle**[c], **Wenjin Xu**[a], **Yunan Yang**[b], **Yin Zhang**[c], **Todd E. Barnhart**[c], **Weibo Cai**[b,c,d,*], and **Shaoqin Gong**[a,**]

[a]Department of Biomedical Engineering and Wisconsin Institutes for Discovery, University of Wisconsin–Madison, Madison, WI 53706, USA

[b]Department of Radiology, University of Wisconsin–Madison, Madison, WI 53705, USA

[c]Department of Medical Physics, University of Wisconsin–Madison, Madison, WI 53705, USA

[d]University of Wisconsin Carbone Cancer Center, Madison, WI 53705, USA

Abstract

A multifunctional unimolecular micelle made of a hyperbranched amphiphilic block copolymer was designed, synthesized, and characterized for cancer-targeted drug delivery and non-invasive positron emission tomography (PET) imaging in tumor-bearing mice. The hyperbranched amphiphilic block copolymer, Boltorn® H40-poly(L-glutamate-hydrazone-doxorubicin)-*b*-poly(ethylene glycol) (i.e., H40-P(LG-Hyd-DOX)-*b*-PEG), was conjugated with *cyclo(Arg-Gly-Asp-D-Phe-Cys)* peptides (cRGD, for integrin $\alpha_v\beta_3$ targeting) and macrocyclic chelators (*1,4,7-triazacyclononane-N, N′, N″-triacetic acid* [NOTA], for ^{64}Cu-labeling and PET imaging) (i.e., H40-P(LG-Hyd-DOX)-*b*-PEG-OCH_3/cRGD/NOTA, also referred to as H40-DOX-cRGD). The anti-cancer drug, doxorubicin (DOX) was covalently conjugated onto the hydrophobic segments of the amphiphilic block copolymer arms (i.e., PLG) via a pH-labile hydrazone linkage to enable pH-controlled drug release. The unimolecular micelles exhibited a uniform size distribution and pH-sensitive drug release behavior. cRGD-conjugated unimolecular micelles (i.e., H40-DOX-cRGD) exhibited a much higher cellular uptake in U87MG human glioblastoma cells due to integrin $\alpha_v\beta_3$-mediated endocytosis than non-targeted unimolecular micelles (i.e., H40-DOX), thereby leading to a significantly higher cytotoxicity. In U87MG tumor-bearing mice, H40-DOX-cRGD-^{64}Cu also exhibited a much higher level of tumor accumulation than H40-DOX-^{64}Cu, measured by non-invasive PET imaging and confirmed by biodistribution studies and *ex vivo* fluorescence imaging. We believe that unimolecular micelles formed by hyperbranched amphiphilic block copolymers that synergistically integrate passive and active tumor-targeting abilities with pH-controlled drug release and PET imaging capabilities provide the basis for future cancer theranostics.

☆*Editor's Note*: This paper is one of a newly instituted series of scientific articles that provide evidence-based scientific opinions on topical and important issues in biomaterials science. They have some features of an invited editorial but are based on scientific facts, and some features of a review paper, without attempting to be comprehensive. These papers have been commissioned by the Editor-in-Chief and reviewed for factual, scientific content by referees.

*Corresponding author. Tel.: +1 608 262 1749. **Corresponding author. Department of Biomedical Engineering and Wisconsin Institutes for Discovery, University of Wisconsin-Madison, Madison, WI 53715, USA. Tel.: +608 316 4311. WCai@uwhealth.org (W. Cai), sgong@engr.wisc.edu (S. Gong).

[1]Contributed equally.

Keywords

Unimolecular micelles; Drug delivery; Theranostic nanocarriers; Hyperbranched amphiphilic block; copolymer; Positron emission tomography (PET); Cyclic arginine-glycine-aspartic acid (cRGD); peptide

1. Introduction

Recent advances in nanotechnology have led to the development of multifunctional nanoparticles with desirable properties that can overcome the limitations of traditional diagnostic and therapeutic agents [1–7]. Nanoparticles that combine therapeutic agents, molecular targeting, and diagnostic imaging capabilities are emerging as the next generation of multifunctional nanomedicine to improve the therapeutic outcome of cancer therapy [6–13]. Among the many nanoparticle systems, polymer micelles (i.e., self-assembled nanoparticles from amphiphilic block copolymers) have attracted significant attention in biomedical research [11,13–15]. Polymer micelles exhibit a unique core–shell architecture where the hydrophobic core serves as a natural carrier environment for hydrophobic drugs and the hydrophilic shell imparts particle stability in an aqueous solution [11,13,16–20].

However, conventional multi-molecular polymer micelles formed by self-assembly of multiple amphiphilic block copolymers tend to exhibit insufficient *in vivo* stability because the stability of multi-molecular polymer micelles is affected by many factors including the concentration of the amphiphilic block copolymers *in vivo*, the various interactions between polymer micelles and serum proteins, flow stress, temperature, ionic strength, etc. For instance, self-assembled multi-molecular polymer micelles are only thermodynamically stable above the critical micelle concentration (CMC) of the amphiphilic molecules [21,22]. Premature disassociation of the self-assembled multi-molecular polymer micelles during circulation in the bloodstream can cause a burst release of high concentration anti-cancer drugs in the bloodstream, which not only leads to potential systemic toxicity but also surrenders the tumor-targeting ability provided by the drug nanocarriers through the enhanced permeability and retention (EPR) effect (i.e., passive tumor-targeting), thereby severely limiting their use for *in vivo* applications.

To improve the thermodynamic instability associated with self-assembled nanoparticles, including polymer micelles and vesicles, various strategies have been investigated including crosslinking the core or shell or both core and shell of the self-assembled nano-carriers, as well as the development of unimolecular micelles [23,24]. While crosslinking the nanocarriers is a very effective approach to ensure excellent *in vivo* stability, it can also lead to a reduced biodegradability and a slower drug release rate, which may not be desirable for *in vivo* drug/agent delivery applications. Unimolecular micelles, formed by single multi-arm star amphiphilic block copolymers having a sufficient number of arms and proper hydrophobic to hydrophilic ratios, can provide excellent *in vivo* stability due to their covalent nature without compromising the biodegradability or drug release profile [22,25–28]. Various types of nanostructures including dendrimers, hyperbranched polymers, and functionalized inorganic nanoparticles can be used as the inner core and/or macroinitiators for the conjugation/synthesis of the amphiphilic block copolymer arms [26–29]. Boltorn H40 (H40), a hyperbranched aliphatic polyester, has received much attention in the design of unimolecular micelles because of its biodegradability, biocompatibility, globular architecture, and a large number of terminal functional groups [22,26–28].

Molecular imaging has been widely used for cancer detection and staging, as well as evaluating the *in vivo* biodistribution of various nanoparticles/nanocarriers [2,30–32].

Among all molecular imaging modalities, positron emission tomography (PET) imaging has become increasingly popular in both preclinical and clinical settings as it offers excellent tissue penetration, higher detection efficiency, non-invasiveness, and superb quantitative accuracy [33]. In particular, PET imaging can be used to provide real-time, non-invasive, and quantitative monitoring of the biodistribution, pharmacokinetics, and tumor-targeting efficacy of the drug nano-carriers, thereby allowing physicians to predict their therapeutic effects. As such, PET-based theranostic nanomedicine has been a dynamic research area over the last several years [3,34–39].

The formation of new blood vessels, or angiogenesis, is an essential component of tumor growth without which a tumor cannot grow beyond a few millimeters in diameter [40–42]. The $\alpha_v\beta_3$ integrin, which plays a pivotal role in both tumor development and tumor metastasis, is over-expressed on both the angiogenic endothelial cells and tumor cells of many types of solid tumors such as melanoma, glioblastoma, breast, prostate, and ovarian cancer [38]. In addition, $\alpha_v\beta_3$ integrin is up-regulated in tumors following radiotherapy [43]. Strategies to simultaneously kill the tumor neovasculature as well as the tumor cells are highly desirable for targeted cancer therapy. It was shown that (1) cRGD ligands can effectively target $\alpha_v\beta_3$ integrin-expressing tumor neovasculature and/or cells, and (2) cRGD-conjugated nanocarriers are internalized by integrin-mediated endocytosis [13,39,44–47].

Herein, we describe the design, synthesis, and characterization of a multifunctional unimolecular micelle system for cancer-targeted PET imaging and drug delivery *in vivo*. The unimolecular micelle was made from a hyperbranched amphiphilic block copolymer, Boltorn® H40-poly(L-glutamate-hydrazone-doxorubicin)-*b*-poly(ethylene glycol) (i.e., H40-P(LG-Hyd-DOX)-*b*-PEG) that was conjugated with *cyclo(Arg-Gly-Asp-D-Phe-Cys)* peptides (cRGD) and macrocyclic chelators (i.e., *1,4,7-triazacyclononane-N, N′, N″-triacetic acid* [NOTA]) (i.e., H40-P(LG-Hyd-DOX)-*b*-PEG-OCH_3/cRGD/NOTA or H40-DOX-cRGD for brevity) (cf. Fig. 1). DOX, a model anti-cancer drug, was conjugated onto the nanocarriers via a pH-sensitive hydrazone bond to enable pH-controlled release, a property desirable for targeted cancer therapy. The cRGD peptides and NOTA, a macrocyclic chelator for ^{64}Cu ($t_{1/2}$: 12.7 h) [12], were selectively conjugated onto the distal ends of the PEG arms. As described above, cRGD peptides enable integrin $\alpha_v\beta_3$-targeting on both the tumor vasculature and tumor cells [37,38]. Complexation of ^{64}Cu onto the unimolecular micelle via NOTA makes PET imaging possible which can provide non-invasive and quantitative measurement of the *in vivo* biodistribution and tumor-targeting efficacy of the H40-based nanocarriers in a U87MG tumor model in living mice.

2. Materials and methods

2.1. Materials

Boltorn H40 (a hyperbranched polyester with 64 hydroxyl terminal groups per molecule; M_n: 2833 Da) was provided by Perstorp Polyols Inc., USA, and purified with acetone and tetrahydrofuran (THF). γ-benzyl-L-glutamate (BLG), triphosgene, succinic anhydride, 4-dimethylamino pyridine (DMAP), N-hydroxysuccinimide (NHS), 1,3-dicyclohexylcarbodiimide (DCC), aminoethanethiol hydrochloride (AET·HCl), and anhydrous hydrazine were purchased from Sigma-Aldrich (Milwaukee, WI, USA) and used without further purification. THF, triethylamine (TEA), dimethyl sulfoxide (DMSO), and dimethylformamide (DMF) were purchased from Sigma-Aldrich (Milwaukee, WI, USA) and were distilled before use. The heterobifunctional PEG derivative, R (R = maleimide (Mal) or methoxy (-OCH_3))-PEG_{114}-NH_2 (Mw = 5000) was acquired from JenKem Technology (Allen, TX, USA). Doxorubicin hydrochloride (DOX·HCl) (Tecoland Corporation, Irvine, CA, USA), cyclo(Arg-Gly-Asp-D-Phe-Cys) (cRGDfC, abbreviated as cRGD), (Peptides International, Louisville, KY, USA), p-SCN–-Bn-NOTA (Macrocyclics,

Inc., Dallas, TX, USA), DMEM (Gibco BRL, Carlsbad, CA, USA), and PD-10 desalting columns (GE Healthcare, Piscataway, NJ, USA) were all commercially available. U87MG human glioblastoma cells (expressing high levels of integrin $\alpha_v\beta_3$ [39,46] were purchased from ATCC and cultured in DMEM supplemented with 10% fetal bovine serum. All other chemicals and reagents used were of analytical reagent grade. Phosphate and acetate buffered solutions were prepared fresh in our laboratory. Ultrapure deionized water (DI water, Milli-Q Water Systems) was used for all buffer solutions and experiments. ^{64}Cu was produced via a ^{64}Ni(p,n)^{64}Cu reaction using a cyclotron at the University of Wisconsin–Madison. During ^{64}Cu-labeling, water and all buffers used were of Millipore grade and pre-treated with Chelex 100 resin (50–100 mesh, Sigma-Aldrich, St. Louis, MO, USA) to ensure that the aqueous solution was free of heavy metals.

2.2. Synthesis of γ-benzyl-L-glutamate-N-carboxyanhydride (BLG-NCA)

BLG (1.5 g, 6.3 mmol) was suspended in 10 ml of anhydrous THF. Triphosgene (0.93 g, 3.2 mmol) in 1 ml anhydrous THF was slowly added to this solution over a period of 30 min. The reaction mixture was stirred at 55 °C under N_2 for 3 h until a clear solution was obtained. The solvent was removed under vacuum and the product was purified by crystallization in a mixed solvent of THF and hexane.

2.3. Synthesis of carboxyl-functionalized H40 (H40-COOH)

H40-COOH was prepared by mixing 1.0 g of H40 (23 mmol of hydroxyl groups) with 2.5 g (45 mmol) of succinic anhydride. The reaction was carried out in the mixture of TEA (0.25 ml) and anhydrous THF (25 ml) for 24 h at room temperature under constant stirring. Subsequently, the precipitate was collected by filtration, thoroughly washed with THF and diethyl ether, and dried under vacuum.

2.4. Synthesis of poly(γ-benzyl-L-glutamate)-b-poly(ethylene glycol) copolymers (PBLG-b-PEG-Mal or PBLG-b-PEG-OCH_3)

Eighty milligrams (mg) (0.30 mmol) of BLG-NCA was dissolved in 6 ml of anhydrous DMF at room temperature. Afterwards, 100 mg (0.02 mmol) of methoxy-PEG-NH_2 (MPEG-NH_2) (or Mal-PEG-NH_2) in 4 ml of DMF was added to the solution. The reaction mixture was stirred at 55 °C under N_2 for 72 h and poured into a 10-fold volume of diethyl ether at 0 °C. The precipitate was collected by filtration, washed with diethyl ether, and dried under vacuum.

2.5. Synthesis of H40-PBLG-b-PEG-OCH_3/Mal

H40-PBLG-*b*-PEG-OCH_3/Mal was synthesized by reacting 12.5 mg (0.001 mmol) of H40-COOH with 204.0 mg (0.024 mmol) of PBLG-*b*-PEG-Mal and 130.5 mg (0.016 mmol) of PBLG-*b*-PEG-OCH_3 in 100 ml of anhydrous DMF, using 13.2 mg (0.064 mmol) of DCC and 7.36 mg (0.064 mmol) of NHS as the coupling reagents. The reaction mixture was stirred at room temperature for 12 h and the by-product, dicyclohexylurea, was removed by filtration. The product, H40-PBLG-*b*-PEG-O CH_3/Mal, was dialyzed against DMF for 48 h using a cellulose dialysis membrane (molecular weight cut-off, 12 kDa). Subsequently, the solution was added into cold diethyl ether to collect the product as a precipitate, which was dried under vacuum.

2.6. Synthesis of H40-P(LG-Hydrazone (Hyd)-DOX)-b-PEG-OCH_3/Mal

The benzyl groups of H40-PBLG-*b*-PEG-OCH_3/Mal were converted to hydrazide groups by reacting 1.77 g H40-PBLG-*b*-PEG-OCH_3/Mal (0.2 mmol of PBLG-*b*-PEG “arms”) with 200 μl anhydrous hydrazine (6 mmol) in dry DMF at 40 °C for 24 h. Thereafter, H40-P(LG-hydrazide)-*b*-PEG-OCH_3/Mal was dialyzed against 0.25% ammonia solution for 48 h,

followed by freeze drying. H40-P(LG-hydrazide)-*b*-PEG-OCH_3/Mal (1.6 g, 0.2 mmol of P(LG-hydrazide)-*b*-PEG "arms") was then dissolved in freshly distilled DMF, and an excess amount of DOX (1.7 g, 3.12 mmol) was added. The mixture was stirred at room temperature for 24 h while being protected from light to obtain H40-P(LG-Hyd-DOX)-*b*-PEG-OCH_3/Mal, which was purified by dialysis against DI water for 48 h to completely remove unreacted DOX. The absence of free DOX was confirmed by thin layer chromatography(TLC).

2.7. Synthesis of H40-P(LG-Hyd-DOX)-b-PEG-OCH_3/cRGD/NOTA

NOTA-SH was prepared via the reaction between the NCS group of p-SCN-Bn-NOTA (56 mg, 0.1 mmol) and the amino group of AET·HCl (11.36 mg, 0.1 mmol) in the presence of TEA in DI water for 6 h at room temperature. Afterwards, a predetermined amount of cRGD (17.4 mg, 0.03 mmol) and NOTA-SH (9.3 mg, 0.015 mmol) were added into an aqueous solution of H40-P(LG-Hyd-DOX)-*b*-PEG-OCH_3/Mal (1 g, 0.003 mmol). The molar ratio for cRGD and NOTA-SH was set at 40% and 20%, respectively, with the total amount (i.e., 60%) equal to that of the PEG-Mal attached to the hyperbranched H40-P(LG-Hyd-DOX)-*b*-PEG-OCH_3/Mal copolymer. The reaction was carried out in an aqueous solution for 6 h at room temperature under N_2 and the product was purified by dialysis with DI water for 48 h. To study the effects of cRGD targeting ligands on cellular uptake and *in vivo* biodistribution, hyperbranched amphiphilic block copolymer H40-P(LG-Hyd-DOX)-*b*-PEG-OCH_3/NOTA (without the cRGD tumor-targeting ligand, i.e., non-targeted) was synthesized following the same procedures as described for the synthesis of H40-P(LG-Hyd-DOX)-*b*-PEG-OCH_3/cRGD/NOTA except that the molar ratio between PEG-Mal and PEG-OCH_3 was reduced proportionally.

2.8. Preparation of H40-P(LG-Hyd-DOX)-b-PEG-OCH_3/cRGD/NOTA micelles

Hyperbranched H40-P(LG-Hyd-DOX)-*b*-PEG-OCH_3/cRGD/NOTA copolymer (50 mg) was dissolved in 5 ml of DMF, to which 15 ml of DI water was added dropwise. The solution was then dialyzed with Millipore water using a cellulose dialysis tubing (molecular weight cut-off, 2 kDa) for 96 h, followed by freeze drying. To determine the drug conjugation level, a weighed quantity (25 mg) of H40-P(LG-Hyd-DOX)-*b*-PEG-OCH_3/cRGD/NOTA was treated with 0.1 N HCl at room temperature for 48 h under constant stirring. After centrifugation, DOX in the supernatant was assayed by a UV–visible spectrophotometer at the wavelength of 485 nm. All experiments were carried out in triplicate. To simplify the notations of these unimolecular micelles, cRGD-conjugated unimolecular micelles formed by hyper-branched H40-P(LG-Hyd-DOX)-*b*-PEG-OCH_3/cRGD/NOTA copolymer will be referred to as "H40-DOX-cRGD" in the remaining text. Likewise, non-targeted unimolecular micelles formed by hyperbranched H40-P(LG-Hyd-DOX)-*b*-PEG-OCH_3/NOTA copolymer will be referred to as "H40-DOX."

2.9. Characterization

^{1}H NMR spectra of all intermediate and final polymer products were recorded at 25 °C on a Bruker DPX 300 spectrometer using D_2O, $CDCl_3$, and DMSO as the solvent. The molecular weight of the polymers was determined by gel permeation chromatography (GPC) with a refractive index detector, a viscometer detector, and a light scattering detector (Viscotek, USA). THF was used as a mobile phase with a flow rate of 1 ml/min. Absorbance measurements were carried out using a Varian Cary 300 Bio UV–visible spectrophotometer. The calibration curve of absorbance for different concentrations of DOX was determined at 485 nm. The hydrodynamic size and size distribution of the unimolecular micelles were determined by dynamic light scattering (DLS) (ZetaSizer Nano ZS90, Malvern Instrument, USA), at a polymer concentration of 0.05 mg/ml. The morphology and size of the dried unimolecular micelles were measured using a transmission electron microscopy (TEM)

(LEO912-OMEGA, Zeiss, Germany). To prepare the TEM sample, a drop of micelle solution (0.05 mg/ml) containing 1 wt.% of phosphotungstic acid was deposited onto a 200 mesh copper grid coated with carbon and dried at room temperature. The DOX loading content (DLC), defined as the weight percentage of DOX in the H40 nano-carriers, was quantified by UV–Vis analysis. First, DOX was released completely from the nanocarriers in a solution of 0.1 N HCl to cleave the hydrazone bonds. The absorbance of DOX at 485 nm was measured to determine the DLC in the solution using a previously established calibration curve. The DLC measurements were performed in triplicate for each sample.

2.10. In vitro drug release study

Drug release studies were performed in a glass apparatus at 37 °C in acetate buffer (pH 5.3 and 6.6) and phosphate buffer (pH 7.4) solutions. 50 mg of H40-DOX-cRGD micelles was dispersed in 5 ml of medium and placed in a dialysis bag with a molecular weight cut-off of 2 kDa. The dialysis bag was immersed in 95 ml of the release medium and kept in a horizontal laboratory shaker (100 rpm) under constant temperature. Samples of 2 ml volume were periodically removed and the same volume of fresh medium was added. The amount of released DOX was analyzed with a spectrophotometer at 485 nm. The drug release studies were performed in triplicate for each sample.

2.11. Cellular uptake study

The cellular uptake behavior and intracellular distribution of the H40-based unimolecular micelles were analyzed using both flow cytometry and confocal laser scanning microscopy (CLSM). For flow cytometry, U87MG cells were seeded in 6-well culture plates and cultured in DMEM overnight. After digestion with 0.05% trypsin, the cells (5×10^6 per ml) were treated with free DOX, H40-DOX-cRGD, or H40-DOX (all with a DOX concentration of 20 μg/ml) for 15 and 120 min in a binding buffer (20 mmol/l Tris, 150 mmol/L NaCl, 2 mmol/l $CaCl_2$, 1 mmol/l $MgCl_2$, 1 mmol/l $MnCl_2$, 0.10% bovine serum albumin, pH 7.4). For the 120-min measurement, a blocking experiment with 2 μM of free cRGD peptide was also carried out for H40-DOX-cRGD. DOX uptake was analyzed by a BD FACSCalibur four-color analysis cytometer (Becton Dickinson, San Jose, CA, USA) and FlowJo analysis software (Tree Star, Inc., Ashland, OR, USA). A minimum of 1×10^4 cells were analyzed from each sample with the DOX fluorescence intensity displayed on a four-decade log scale.

For CLSM studies, U87MG cells (1×10^6 per well) were seeded onto 35 mm round micro-dishes (ibidi LLC, Verona, WI) and cultured overnight. Cells were treated with free DOX, H40-DOX-cRGD, H40-DOX-cRGD with cRGD blocking, or H40-DOX for 120 min (DOX concentration: 20 μg/ml). After incubation, the cells were washed with PBS and fixed with cold acetone. DOX uptake was analyzed using a Nikon A1R-Si high speed spectral laser scanning confocal inverted microscope (Nikon, Melville, NY). Digital monochromatic images were acquired using NIS-Elements BR Software.

2.12. Cytotoxicity assay

The cytotoxicity of free DOX, H40-DOX, and H40-DOX-cRGD to U87MG cells was studied using the MTT assay. In brief, U87MG cells (1×10^4) were seeded in 96-well plates and incubated overnight in DMEM. The media was replaced with fresh media containing free DOX, H40-DOX, or H40-DOX-cRGD at different DOX concentrations (10, 20, and 40 μg/ml) and incubated for 48 h. Cells grown in pure culture medium served as a 100% cell viability control. Afterwards, cells were washed twice with PBS and 0.2 ml of MTT solution (0.5 mg/ml in DMEM) was added to each well. The plate was then incubated for 4 h at 37 °C to allow MTT metabolism. Subsequently,150 μl of DMSO was added to each well and the plate was incubated for 30 min at room temperature. The absorbance at 570 nm was measured with a Spectramax Plus384 absorbance microplate reader (Molecular Devices,

Sunnyvale, CA), with an absorbance of 630 nm used as the reference. The net A_{570}–A_{630} was taken as the index of cell viability.

2.13. Animal model

All animal studies were conducted under a protocol approved by the University of Wisconsin Institutional Animal Care and Use Committee. U87MG cells were used for tumor inoculation when they reached ~80% confluence. Four- to five-week-old female athymic nude mice were purchased from Harlan (Indianapolis, IN) and tumors were established by subcutaneously injecting 5×10^6 cells, suspended in 100 μl of 1:1 mixture of medium and matrigel (BD Biosciences, Franklin lakes, NJ), into the front flank of the mice [48]. The tumor sizes were monitored every other day and the animals were subjected to *in vivo* experiments when the diameter of the tumors reached 6–8 mm (typically 4 weeks after inoculation).

2.14. ^{64}Cu-labeling of H40-DOX and H40-DOX-cRGD

^{64}Cu-labeling was performed in a manner similar to our previous studies [12,49]. In brief, $^{64}CuCl_2$ (74 MBq) was diluted in 300 μl of 0.1 M sodium acetate buffer (pH 6.5) and added to the H40-DOX or H40-DOX-cRGD solution containing approximately 2 μg of NOTA. The reaction mixture was incubated for 30 min at 42 °C with constant shaking. The H40-DOX-^{64}Cu or H40-DOX-cRGD-^{64}Cu was purified using PD-10 columns with PBS as the mobile phase before animal studies.

2.15. Imaging and biodistribution studies

PET and PET/CT scans at various time points post-injection (p.i.), image reconstruction, and region-of-interest (ROI) analysis were performed using a microPET/microCT Inveon rodent model scanner (Siemens Medical Solutions USA, Inc.) as described previously [12,50,51]. Each tumor-bearing mouse was injected with 5–10 MBq of H40-DOX-cRGD-^{64}Cu or H40-DOX-^{64}Cu via the tail vein and 3–15 min static PET scans were performed. Quantitative data were presented as percentage injected dose per gram of tissue (%ID/g). Three U87MG tumor-bearing mice were co-injected with 10 mg/kg dose of cRGD peptide and H40-DOX-cRGD-^{64}Cu to evaluate the target specificity ofH40-DOX-cRGD-^{64}Cu *invivo*. Biodistribution studies were carried out after the last PETscans to validate the PET results. The radioactivity in the tissue was measured using a gamma-counter (Perkin Elmer) and presented as %ID/g (mean ± SD).

2.16. Ex vivo fluorescence imaging

To confirm that DOX from H40-DOX-cRGD-^{64}Cu or H40-DOX-^{64}Cu was indeed delivered to the U87MG tumors, *ex vivo* fluorescence imaging was carried out. Fluorescence images were acquired with an IVIS spectrum system (Caliper Life Sciences, Hopkinton, MA) with an excitation maximum of 465 nm and emission maximum of 560 nm. U87MG tumors from mice which did not receive any injections were also scanned and used for background fluorescence subtraction.

3. Results and discussion

3.1. Synthesis and characterization of H40-DOX and H40-DOX-cRGD

Syntheses of H40-DOX and H40-DOX-cRGD were carried out as shown in Scheme 1. First, copolymers of PBLG-*b*-PEG-Mal and PBLG-*b*-PEG-OCH_3 were prepared by ring-opening polymerization of BLG-NCA in anhydrous DMF, using Mal-PEG-NH_2 and OCH_3-PEG-NH_2 as macroinitiators, respectively. The formation of the two copolymers was confirmed by ^{1}H NMR (Fig. 2A). The peaks at 7.21–7.30 ppm and 5.10 ppm are ascribed to the

protons in the benzyl and -CH_2 groups in the PBLG side chains, respectively. The signal at 2.03–2.46 ppm corresponds to the -CH_2CH_2- groups of the side chain that connects to the main chain of PBLG (i.e., -$CHCH_2CH_2COO$-). The peak at 3.65 ppm was originated from the methylene protons within PEG. According to the ^{1}H NMR spectrum, the number average molecular weight (M_n) of PBLG-b-PEG-Mal was 7206, which was calculated based on the relative intensity ratio of the CH_2 proton of the PEG chain (-OCH_2CH_2, d = 3.65) and the CH_2 proton next to the benzyl group of the PBLG chain (-$COOCH_2C_6H_5$, d = 5.10). The M_n of PBLG-b-PEG-Mal determined by ^{1}H NMR was consistent with that obtained by the GPC measurement (Table 1).

In the next step, the -COOH groups of H40-COOH were reacted with the NH_2 group of PBLG-*b*-PEG-Mal and PBLG-*b*-PEG-OCH_3 to form hyperbranched amphiphilic H40-PBLG-*b*-PEG-OCH_3/Mal copolymer via the amide linkage. Based on our previous study for the SPIO nanocarriers [12], the feed molar ratio of PBLG-*b*-PEG-Mal and PBLG-*b*-PEG-OCH_3 was set at 3:2 (corresponding to 60% PEG-Mal terminal groups and 40% PEG-OCH_3 terminal groups in molar ratio). The Mal terminal groups present in PEG-Mal were used for cRGD and NOTA conjugation; and the -OCH_3 groups present in PEG-OCH_3 were used to help control the molar ratio of maleimide at the micelle surface, which subsequently controls the density of cRGD and NOTA. The coupling reaction was carried out in dry DMF at room temperature in the presence of DCC as the activating agent for the carboxylic group and NHS. The product was purified by dialysis against DMF (molecular weight cut-off, 12 kDa) to eliminate the unreacted PBLG-*b*-PEG-Mal and PBLG-*b*-PEG-OCH_3 from the crude H40-PBLG-*b*-PEG-OCH_3/Mal copolymer. In the ^{1}H NMR spectrum of H40-PBLG-*b*-PEG-OCH_3/Mal (Fig. 2B), in addition to the characteristics peaks of the PBLG and PEG blocks, the peaks at 4.32, 3.40–3.62, 2.83, 2.90, and 1.33 ppm were observed due to the methylene and methyl protons of H40-COOH, respectively. These results clearly indicate the formation of the H40-PBLG-*b*-PEG-OCH_3/Mal copolymer. The average number of arms per H40-PBLG-*b*-PEG-OCH_3/Mal molecule was estimated via comparing the molecular weights of H40-COOH, PBLG-*b*-PEG-OCH_3/Mal and H40-PBLG-*b*-PEG-OCH_3/Mal determined by a GPC equipped with triple detectors, as shown in Table 1. The average number of arms per H40-PBLG-*b*-PEG-OCH_3/Mal molecule was estimated to be 25 from the M_w values of H40-COOH, PBLG-*b*-PEG-Mal, PBLG-*b*-PEG-OCH_3, and H40-PBLG-*b*-PEG-OCH_3/Mal using the following equation:

Number of arms = (M_w of H40-PBLG-*b*-PEG-OCH_3/Mal – M_w of H40-COOH)/average M_w of (PBLG-*b*-PEG-Mal and PBLG-*b*-PEG-OCH_3)] = [(220985–12502)/8365] = 25. The average M_w of the PBLG-*b*-PEG-Mal and PBLG-*b*-PEG-OCH_3 was calculated based on their molar ratio (15:10). This finding is consistent with previous reports on the number of arms for H40-based hyperbranched amphiphilic block copolymers [22,26,52].

Next, the model anti-cancer drug, DOX, was conjugated to the H40-PBLG-*b*-PEG-OCH_3/Mal polymer via a two-step reaction [53]. First, the benzyl groups of H40-PBLG-*b*-PEG-OCH_3/Mal were substituted with hydrazide groups to obtain H40-P(LG-hydrazide)-*b*-PEG-OCH_3/Mal by an ester-amide exchange aminolysis (EAE) reaction. In the second step, an excess amount of DOX was conjugated to the hydrazide group of the H40-P(LG-hydrazide)-*b*-PEG-OCH_3/Mal through a pH-sensitive hydrazone linkage. As shown in Fig. 2C, the NMR peaks at 0.82, 1.13–1.47, 4.93, and 7.20–7.92 ppm were originated from DOX indicating that the DOX molecules were successfully conjugated onto the PBLG segments by hydrazone bonds.

Lastly, the cRGD peptide for integrin $\alpha_v\beta_3$-targeting and NOTA for ^{64}Cu chelation were conjugated onto the surface of the H40-P(LG-Hyd-DOX)-*b*-PEG-OCH_3/Mal copolymer through the reaction between the Mal groups on the surface of H40-P(LG-Hyd-DOX)-*b*-

PEG-OCH_3/Mal with the thiol groups of cRGD and/or thiolated NOTA (NOTA-SH) to obtain the final product H40-P(LG-Hyd-DOX)-*b*-PEG-OCH_3/cRGD/NOTA. To conduct the reaction, NOTA-SH was first prepared by reacting p-SCN-Bn-NOTA with aminoethanethiol hydrochloride (AET·HCl) in the presence of TEA. Thereafter, cRGD and NOTA-SH in an aqueous solution was added to the solution of H40-P(LG-Hyd-DOX)-*b*-PEG-OCH_3/Mal suspended in water with the feed molar ratio of cRGD: NOTA: H40-P(LG-Hyd-DOX)-*b*-PEG-OCH_3/Mal at 10: 5: 1. As discussed earlier, there were approximately 25 P(LG-Hyd-DOX)-*b*-PEG-OCH_3/Mal arms per hyperbranched amphiphilic block copolymer, among which 15 arms were conjugated with Mal terminal groups at the distal end of PEG. In order to achieve sufficient targeting efficiency to $\alpha_v\beta_3$-expressing cells while ensuring efficient isotope chelation for PET detection, the molar ratio for cRGD:NOTA was set at 2:1, with the total molar amount being equal to that of Mal-PEG. The NMR spectrum of H40-P(LG-Hyd-DOX)-*b*-PEG-OCH_3/cRGD/NOTA is shown in Fig. 2D. The appearance of a group of overlapping NMR peaks ranging from 7.10 to 8.20 ppm that are attributed to the phenyl protons of DOX, cRGD and NOTA as well as the complete disappearance of the maleimide signal at 6.74 ppm clearly suggested the successful conjugation of cRGD and NOTA to the H40-based amphiphilic block copolymer. Hyperbranched H40-P(LG-Hyd-DOX)-*b*-PEG-OCH_3/NOTA copolymer, which was used to prepare non-targeted (without cRGD) unimolecular micelles, was synthesized in a similar fashion.

3.2. Micellar properties of hyperbranched H40-P(LG-Hyd-DOX)-b-PEG-OCH_3/cRGD/NOTA copolymers

The hyperbranched H40-P(LG-Hyd-DOX)-*b*-PEG-OCH_3/cRGD/NOTA amphiphilic block copolymer can form a stable unimolecular micelle in an aqueous solution due to its large number of amphiphilic arms (~25) with proper hydrophilic to hydrophobic ratios as well as its globular architecture. The hydrophobic H40-P(LG-Hyd-DOX) inner segment forms a hydrophobic core while the hydrophilic PEG-OCH_3/cRGD/NOTA segment forms a hydrophilic shell stabilizing the resulting unimolecular micelle in an aqueous solution. It is well known that the stability and size of drug nanocarriers, including polymer micelles, play an important role in the cellular internalization process as well as their *in vivo* performance. In this study, the stability of the unimolecular micelles prepared from the hyperbranched H40-P(LG-Hyd-DOX)-*b*-PEG-OCH_3/cRGD/NOTA copolymer in an aqueous medium was evaluated by comparing the visual appearance and the average size of the freshly prepared micelles with those of the micelles stored at 4 °C in a PBS solution for one month. It was found that there was no notable change in both the appearance (e.g., no precipitations) and the size of the unimolecular micelles over one month. The size distribution histogram of the H40-DOX-cRGD micelles measured by DLS at a concentration of 0.05 mg/ml is shown in Fig. 3A. The hydrodynamic diameter of the H40-DOX-cRGD micelles ranged from 44 to 91 nm, with an average diameter of 65 nm. Fig. 3B shows the TEM images of the unimolecular micelles which were stained by phosphotungstic acid on a carbon-coated copper grid. As expected, the unimolecular micelles possessed a spherical shape with a diameter ranging from 22 to 31 nm. The size distribution of the micelles was also relatively narrow based on both DLS and TEM analyses. The reason that the sizes of the unimolecular micelles measured by TEM were smaller than that measured by DLS was that DLS measures the hydrodynamic diameters with hydrophilic PEG layers extending into the aqueous solution while the TEM measures the diameter of dried umimolecular micelles.

3.3. Drug loading level and in vitro drug release

The amount of DOX incorporated into the H40 nanocarriers was 16.2 wt.% as measured by UV analysis using DOX's absorption peak at 485 nm after it was cleaved from the H40-based nanocarriers in a 0.1 N HCl solution. To test the pH-sensitivity of H40-DOX-cRGD, *in vitro* drug release studies were performed under simulated physiological and cellular

conditions at pH 5.3, 6.6, and 7.4 at 37 °C. As shown in Fig. 4, the pH value of the medium had a strong effect on the release rate of DOX from the H40-DOX-cRGD. Specifically, the release rate of DOX increased consistently with lower pH values within a pH range of 5.3–7.4. At a pH of 7.4, the amount of DOX released after 45 h was 12.1%, including an initial burst release of about 4.7%. This result suggests that the pH-labile hydrazone linkages between DOX and the H40-DOX-cRGD nanocarriers could be rather stable under physiological conditions. However, at pH values of 5.3 and 6.6, the amount of DOX released was approximately 92.7% and 85.6% after 45 h, respectively, confirming that the DOX release from the H40-DOX-cRGD in an acidic environment was governed by the acid-cleavable hydrazone linkage. As such, the pH-sensitive H40-DOX-cRGD will minimize premature drug release during circulation in the bloodstream (pH 7.4), yet provide a sufficient amount of drug to effectively kill cancer cells once the H40-DOX-cRGD are internalized into the endocytic compartments where the pH value ranges from 4.5 to 6.5. The pH-dependent drug release behavior is very desirable in achieving tumor-targeted DOX delivery using nanocarriers as it would greatly enhance tumor-directed therapeutic efficacy while minimizing any non-specific systemic spread of toxicity. These findings agree with our previous studies on intracellular environment-sensitive drug delivery systems [12,22,26,29,30].

3.4. Cellular uptake and distribution of H40-DOX and H40-DOX-cRGD

Fig. 5 shows the quantitative flow cytometry analysis results of U87MG cellular uptake of free DOX, H40-DOX, and H40-DOX-cRGD at an early (15 min) and late (120 min) time point. Cells without any treatment were used as a negative control, which showed only negligible levels of autofluorescence at both time points. After 15 min, the cellular uptake of H40-DOX-cRGD in U87MG cells was similar to that of free DOX, both of which were significantly higher (>50%) than that of H40-DOX. At 120 min, all treatment groups showed a marked increase in the cellular uptake of DOX. Importantly, cells treated with H40-DOX-cRGD exhibited a 90% higher level of cellular uptake than cells treated with H40-DOX, indicating that cRGD conjugation substantially increased the cellular uptake of the H40-based unimolecular micelles through integrin-mediated endocytosis. The cellular uptake of H40-DOX-cRGD was only slightly lower than that of free DOX, which can readily diffuse across the cell membrane.

To further investigate the effects of cRGD conjugation on the cellular uptake of the H40-based unimolecular micelle, CLSM analysis of U87MG cells was performed to examine the intracellular localization of DOX. As expected, treatment of U87MG cells with free DOX for 120 min led to strong DOX fluorescence in both the cytoplasm and the nucleus (Fig. 6). Cells treated with H40-DOX-cRGD showed a similar level of DOX fluorescence in the cytoplasm but somewhat lower fluorescence in the nucleus. This may be attributed to the fact that DOX conjugated onto the unimolecular micelles via the pH-sensitive hydrazone bond must be first cleaved and then released from the micelles located in the endocytic compartments before entering the cell nucleus. In contrast, cells treated with H40-DOX only showed low-level cytoplasmic and nuclear DOX fluorescence. Blocking with 2 μM of cRGD significantly reduced the cytoplasmic fluorescence intensity of H40-DOX-cRGD, which was even lower than that of H40-DOX. Taken together, CLSM studies confirmed the findings from flow cytometry analysis, namely that cRGD conjugation markedly increased the cellular uptake of H40-based unimolecular micelles in an integrin $\alpha_V\beta_3$ specific manner.

3.5. Cytotoxicity of H40-DOX and H40-DOX-cRGD

To determine the cytotoxicity of H40-DOX and H40-DOX-cRGD, U87MG cells were treated with the unimolecular micelles at varying DOX concentrations (i.e., 10, 20, and 40 μg/ml) for 48 h and analyzed using the MTT assay. Free DOX was used as a control. As

shown in Fig. 7, the cytotoxicity of free DOX was significantly higher than that of H40-DOX-cRGD and H40-DOX because free DOX can quickly diffuse into the cytoplasm and then the nucleus of the U87MG cells. DOX intercalates the DNA thereby preventing its replication. However, free DOX does not have tumor-targeting abilities *in vivo* which can lead to severe side effects. Among the two unimolecular micelles, H40-DOX-cRGD had significantly higher (~15%) cytotoxicity to U87MG cells than H40-DOX ($p < 0.05$) at equivalent DOX concentrations of 20 and 40 μg/ml, confirming that cRGD conjugation increased the cytotoxicity of H40-DOX, which was consistent with the increases in cellular uptake as observed with both flow cytometry and CLSM analyses. In addition, the fact that H40-DOX-cRGD induced substantial cytotoxicity in U87MG cells strongly suggested that a sufficient amount of DOX was released from the unimolecular micelles and entered the cell nucleus prior to this time point.

3.6. In vivo investigation of H40-DOX and H40-DOX-cRGD

Based on our previous studies with ^{64}Cu-labeled nanoparticles [12,54,55], the time points of 0.5, 4, 16, and 24 h p.i. were chosen for PET scans after intravenous injection of H40-DOX-^{64}Cu or H40-DOX-cRGD-^{64}Cu. The coronal slices that contained the U87MG tumors are shown in Fig. 8A and representative microPET/microCT fused images of a mouse at 4 h p.i. of H40-DOX-cRGD-^{64}Cu are shown in Fig. 8B. H40-DOX-cRGD-^{64}Cu primarily accumulated in the liver, tumor, lung, kidney and intestines, but not in most normal tissues (e.g. muscle, bone, brain, etc.), demonstrating good tumor-targeting efficacy and good tumor contrast. In contrast, the tumor accumulation of H40-DOX-^{64}Cu as well as H40-DOX-cRGD-^{64}Cu with a blocking dose of cRGD peptide (10 mg/kg of mouse body weight) was low (Fig. 8A), which was further confirmed by quantitative analysis as discussed below.

Quantitative data obtained from ROI analyses are shown in Fig. 9A–C. Uptake of H40-DOX-cRGD-^{64}Cu in the liver (due to the uptake of the unimolecular micelles in the reticuloendothelial system (RES)) was prominent at early time points, which gradually declined over time. The liver uptake of H40-DOX-cRGD-^{64}Cu was 14.7 ± 1.5, 12.4 ± 1.7, 9.2 ± 0.8, and 8.0 ± 0.5 %ID/g at 0.5, 4, 16, and 24 h p.i., respectively. The U87MG tumor uptake of H40-DOX-cRGD-^{64}Cu was clearly visible at 0.5 h p.i. and dropped slowly after 4 h p.i. (4.1 ± 0.5, 5.7 ± 1.2, 3.7 ± 0.8, and 3.1 ± 0.2 %ID/g at 0.5, 4, 16, and 24 h p.i. respectively; $n = 3$; Fig. 9A). Administrating a blocking dose of cRGD peptide (10 mg/kg of mouse body weight) along with H40-DOX-cRGD-^{64}Cu reduced the tumor uptake significantly (Fig. 9C), which confirmed integrin $\alpha_v\beta_3$ specificity of H40-DOX-cRGD-^{64}Cu *in vivo*. Liver uptake in the blocking group was also significantly higher than H40-DOX-cRGD-^{64}Cu at early time points (0.5 h and 4 h p.i.). Radioactivity in the blood was 1.9 ± 0.5, 2.1 ± 0.6, 2.1 ± 0.8, and 1.6 ± 0.6 %ID/g at 0.5, 4, 16, and 24 h p.i., respectively ($n = 3$, Fig. 9A). The low radioactivity (~2 %ID/g) in the blood pool indicated that the blood half-lives of both H40-based unimolecular micelles were less than 0.5 h. Further optimization on the size, chemical structure, and surface properties of the unimolecular micelles may prolong the circulation time, thereby increasing *in vivo* tumor accumulation.

H40-DOX-^{64}Cu served as a control for investigating the uptake of the H40-based unimolecular micelles in the U87MG tumors due to passive targeting only (i.e., via the enhanced permeability and retention effect). As can be seen in Fig. 9B, the tumor uptake of H40-DOX-^{64}Cu (~2.5 %ID/g) was significantly lower than that of H40-DOX-cRGD-^{64}Cu at time points before 24 h p.i. ($p < 0.05$; $n = 3$), which further confirmed integrin $\alpha_v\beta_3$ specificity of H40-DOX-cRGD-^{64}Cu *in vivo*.

After the last PET scans at 24 h p.i., all mice were euthanized. *Ex vivo* fluorescence imaging of the U87MG tumors revealed a much stronger tumor fluorescence signal of DOX in mice injected with H40-DOX-cRGD-^{64}Cu than those from mice injected with H40-DOX-^{64}Cu

(Fig. 11), which unambiguously confirmed that DOX was delivered to the tumor tissue. In addition, all major organs were collected for biodistribution studies to further validate *in vivo* PET data (Fig. 10). A tumor/muscle ratio of 7.5 ± 1.5 was achieved at 24 h p.i. (n = 3), which gave an excellent tumor contrast. A comparison of the biodistribution data of H40-DOX-cRGD-^{64}Cu and H40-DOX-^{64}Cu at 24 h p.i. revealed that the uptake of H40-DOX-^{64}Cu was similar in most organs except the U87MG tumor (Fig. 10), which again indicated a tumor specificity of H40-DOX-cRGD-^{64}Cu. Furthermore, a comparison of the biodistribution data of H40-DOX-cRGD-^{64}Cu with the blocking group revealed a similar trend (Fig. 10). Overall, the quantification results obtained from biodistribution studies and PET scans matched very well, con-firming that quantitative ROI analysis of non-invasive microPET scans truly reflected the distribution of H40-DOX-cRGD-^{64}Cu and H40-DOX-^{64}Cu *in vivo*.

All nanomaterials, when intravenously injected, cleared through either the hepatobiliary or renal pathway. In the case of our multifunctional unimolecular micelles, the intact nanocarriers (both H40-DOX-cRGD-^{64}Cu and H40-DOX-^{64}Cu) clear through the hepatobiliary pathway since their hydrodynamic diameter is significantly larger than the cut-off for renal filtration (around 5 nm). Over time, a portion of the nanocarriers get metabolized or degraded in mice and some of the small fragments will undergo renal clearance. In addition, although NOTA is one of the most stable chelators for ^{64}Cu, some transchelation may still occur which can lead to both liver and kidney uptake of radioactivity. Therefore, it is not surprising that the clearance organs (e.g., liver, kidney, and intestines) exhibit a prominent radioactivity signal in PET. However, when compared to most other organs that are not related to clearance (e.g. muscle, brain, bone, skin, etc.), the tumor uptake is significantly higher, which demonstrates good tumor-targeting efficacy of H40-DOX-cRGD. At the three early time points, the U87MG tumor uptake of H40-DOX-cRGD is significantly higher than the two control groups based on quantitative analysis of the PET data. At the last time point, when biodistribution studies were carried out to validate the quantitation capability of PET, appreciable clearance of the nanocarriers had already occurred which rendered the difference in tumor uptake statistically insignificant even though the average tumor uptake of H40-DOX-cRGD was higher than the two control groups.

4. Conclusions

Multifunctional unimolecular micelles made of hyperbranched amphiphilic block copolymers conjugated with cRGD and NOTA have been synthesized and characterized for cancer-targeted drug delivery and PET imaging. The hydrodynamic diameter of these unimolecular micelles was 65 nm as measured by DLS. These multifunctional unimolecular micelles exhibited a pH-sensitive drug release behavior due to the acid-labile hydrazone linkage between DOX and the micelles, which can minimize non-specific systemic spread of toxic drugs during circulation while maximizing the efficiency of tumor-targeted drug delivery. cRGD-conjugated unimolecular micelles (i.e., H40-DOX-cRGD, targeted) exhibited a much higher cellular uptake in U87MG human glioblastoma cells due to integrin $\alpha_v\beta_3$-mediated endocytosis than non-targeted unimolecular micelles (i.e., H40-DOX), thereby leading to a significantly higher cytotoxicity. In tumor bearing mice, H40-DOX-cRGD-^{64}Cu also exhibited a much higher level of tumor accumulation than H40-DOX-^{64}Cu, as measured by non-invasive PET imaging and confirmed by biodistribution studies and *ex vivo* fluorescence imaging. Thus, these multifunctional unimolecular micelles possessing passive and active tumor-targeting abilities, pH-controlled drug release, and PET imaging capabilities capabilities are potentially important drug nanocarriers for targeted cancer theranostics.

Acknowledgments

This work was supported, in part, by the National Science Foundation (DMR 1032187, awarded to Gong, S.), the Department of Defense (W81XWH-11-1-0644 and W81XWH-11-1-0648, awarded to Cai, W.), and the NIH through the UW Radiological Sciences Training Program 5 T32 CA009206-32.

References

1. Peer D, Karp JM, Hong S, Farokhzad OC, Margalit R, Langer R. Nanocarriers as an emerging platform for cancer therapy. Nat Nanotechnol. 2007; 2:751–60. [PubMed: 18654426]
2. Cai W, Chen X. Nanoplatforms for targeted molecular imaging in living subjects. Small. 2007; 3:1840–54. [PubMed: 17943716]
3. Hong H, Zhang Y, Sun J, Cai W. Molecular imaging and therapy of cancer with radiolabeled nanoparticles. Nano Today. 2009; 4:399–413. [PubMed: 20161038]
4. van Vlerken LE, Vyas TK, Amiji MM. Poly(ethylene glycol)-modified nano-carriers for tumor-targeted and intracellular delivery. Pharm Res. 2007; 24:1405–14. [PubMed: 17393074]
5. Jain RK, Stylianopoulos T. Delivering nanomedicine to solid tumors. Nat Rev Clin Oncol. 2010; 7:653–64. [PubMed: 20838415]
6. Ferrari M. Cancer nanotechnology: opportunities and challenges. Nat Rev Cancer. 2005; 5:161–71. [PubMed: 15738981]
7. Cabral H, Nishiyama N, Kataoka K. Supramolecular nanodevices: from design validation to theranostic nanomedicine. Acc Chem Res. 2011; 44:999–1008. [PubMed: 21755933]
8. Rosi NL, Mirkin CA. Nanostructures in biodiagnostics. Chem Rev. 2005; 105:1547–62. [PubMed: 15826019]
9. Williams DF. On the nature of biomaterials. Biomaterials. 2009; 30:5897–909. [PubMed: 19651435]
10. Kim K, Kim JH, Park H, Kim YS, Park KS, Nam H, et al. Tumor-homing multi-functional nanoparticles for cancer theragnosis: Simultaneous diagnosis, drug delivery, and therapeutic monitoring. J Control Release. 2010; 146:219–27. [PubMed: 20403397]
11. Nasongkla N, Bey E, Ren J, Ai H, Khemtong C, Guthi JS, et al. Multifunctional polymeric micelles as cancer-targeted, MRI-ultrasensitive drug delivery systems. Nano Lett. 6:2427–2430. [PubMed: 17090068]
12. Yang X, Hong H, Grailer JJ, Rowland IJ, Javadi A, Hurley SA, et al. cRGD-functionalized, DOX-conjugated, and ^{64}Cu-labeled superparamagnetic iron oxide nanoparticles for targeted anticancer drug delivery and PET/MR imaging. Biomaterials. 2011; 32:4151–60. [PubMed: 21367450]
13. Nasongkla N, Shuai XT, Ai H, Weinberg BD, Pink J, Boothman DA, et al. cRGD-functionalized polymer micelles for targeted doxorubicin delivery. Angew Chem Int Ed Engl. 2004; 43:6323–7. [PubMed: 15558662]
14. Oerlemans C, Bult W, Bos M, Storm G, Nijsen JF, Hennink WE. Polymeric micelles in anticancer therapy: targeting, imaging and triggered release. Pharm Res. 2010; 27:2569–89. [PubMed: 20725771]
15. Torchilin VP. Micellar nanocarriers: pharmaceutical perspectives. Pharm Res. 2007; 24:1–16. [PubMed: 17109211]
16. Gao GH, Lee JW, Nguyen MK, Im GH, Yang J, Heo H, et al. pH-responsive polymeric micelle based on PEG-poly(β-amino ester)/(amido amine) as intelligent vehicle for magnetic resonance imaging in detection of cerebral ischemic area. J Control Release. 2011; 155:11–7. [PubMed: 20854855]
17. Yokoyama M. Polymeric micelles as a new drug carrier system and their required considerations for clinical trials. Expert Opin Drug Deliv. 2010; 7:145–58. [PubMed: 20095939]
18. Mishra D, Kang HC, Bae YH. Reconstitutable charged polymeric (PLGA)(2)-b-PEI micelles for gene therapeutics delivery. Biomaterials. 2011; 32:3845–54. [PubMed: 21354616]
19. Blanco E, Bey EA, Khemtong C, Yang SG, Setti-Guthi J, Chen HB, et al. β-lapachone micellar nanotherapeutics for non-small cell lung cancer therapy. Cancer Res. 2010; 70:3896–904. [PubMed: 20460521]

20. Wei H, Zhang XZ, Zhou Y, Cheng SX, Zhuo RX. Self-assembled thermoresponsive micelles of poly(N-isopropylacrylamide-b-methyl methacrylate). Biomaterials. 2006; 27:2028–34. [PubMed: 16225918]
21. Hall, DG.; Pethica, BA. Thermodynamics of micelle formation. In: Schick, MJ., editor. Nonionic surfactants. New York: Marcel Dekker; 1967. p. 516-57.
22. Prabaharan M, Grailer JJ, Pilla S, Steeber DA, Gong SQ. Amphiphilic multi-arm-block copolymer conjugated with doxorubicin via pH-sensitive hydrazone bond for tumor-targeted drug delivery. Biomaterials. 2009; 30:5757–66. [PubMed: 19643472]
23. Nishiyama N, Kataoka K. Current state, achievements, and future prospects of polymeric micelles as nanocarriers for drug and gene delivery. Pharmacol Ther. 2006; 112:630–48. [PubMed: 16815554]
24. Talelli M, Iman M, Varkouhi AK, Rijcken CJ, Schiffelers RM, Etrych T, et al. Core-crosslinked polymeric micelles with controlled release of covalently entrapped doxorubicin. Biomaterials. 2010; 31:7797–804. [PubMed: 20673684]
25. Kim S, Shi YZ, Kim JY, Park K, Cheng JX. Overcoming the barriers in micellar drug delivery: loading efficiency, *in vivo* stability, and micelle-cell interaction. Expert Opin Drug Deliv. 2010; 7:49–62. [PubMed: 20017660]
26. Prabaharan M, Grailer JJ, Pilla S, Steeber DA, Gong SQ. Folate-conjugated amphiphilic hyperbranched block copolymers based on Boltorn H40, poly(L-lactide) and poly(ethylene glycol) for tumor-targeted drug delivery. Biomaterials. 2009; 30(16):3009–19. [PubMed: 19250665]
27. Li XJ, Qian YF, Liu T, Hu XL, Zhang GY, You YZ, et al. Amphiphilic multiarm star block copolymer-based multifunctional unimolecular micelles for cancer targeted drug delivery and MR imaging. Biomaterials. 2011; 32:6595–605. [PubMed: 21663960]
28. Pang Y, Liu JY, Su Y, Zhu BS, Huang W, Zhou YF, et al. Bioreducible unimolecular micelles based on amphiphilic multiarm hyperbranched copolymers for triggered drug release. Sci China-Chem. 2010; 53:2497–508.
29. Prabaharan M, Grailer JJ, Pilla S, Steeber DA, Gong SQ. Gold nanoparticles with a monolayer of doxorubicin-conjugated amphiphilic block copolymer for tumor-targeted drug delivery. Biomaterials. 2009; 30:6065–75. [PubMed: 19674777]
30. Yang X, Grailer JJ, Rowland IJ, Javadi A, Hurley SA, Matson VZ, et al. Multi-functional stable and pH-responsive polymer vesicles formed by hetero-functional triblock copolymer for targeted anticancer drug delivery and ultrasensitive MR imaging. ACS Nano. 2010; 4:6805–17. [PubMed: 20958084]
31. Massoud TF, Gambhir SS. Molecular imaging in living subjects: seeing fundamental biological processes in a new light. Genes Dev. 2003; 17:545–80. [PubMed: 12629038]
32. Weissleder R, Pittet MJ. Imaging in the era of molecular oncology. Nature. 2008; 452:580–9. [PubMed: 18385732]
33. Phelps ME. PET: the merging of biology and imaging into molecular imaging. J Nucl Med. 2000; 41:661–81. [PubMed: 10768568]
34. Petersen AL, Binderup T, Rasmussen P, Henriksen JR, Elema DR, Kjaer A, et al. ^{64}Cu loaded liposomes as positron emission tomography imaging agents. Biomaterials. 2011; 32:2334–41. [PubMed: 21216003]
35. Burns AA, Vider J, Ow H, Herz E, Penate-Medina O, Baumgart M, et al. Fluorescent silica nanoparticles with efficient urinary excretion for nanomedicine. Nano Lett. 2009; 9:442–8. [PubMed: 19099455]
36. Xie J, Chen K, Huang J, Lee S, Wang JH, Gao JH, et al. PET/NIRF/MRI triple functional iron oxide nanoparticles. Biomaterials. 2010; 31:3016–22. [PubMed: 20092887]
37. Cai W, Chen X. Multimodality molecular imaging of tumor angiogenesis. J Nucl Med. 2008; 49(Suppl 2):113S–28S. [PubMed: 18523069]
38. Cai W, Niu G, Chen X. Imaging of integrins as biomarkers for tumor angiogenesis. Curr Pharm Des. 2008; 14:2943–73. [PubMed: 18991712]
39. Cai W, Shin DW, Chen K, Gheysens O, Cao Q, Wang SX, et al. Peptide-labeled near-infrared quantum dots for imaging tumor vasculature in living subjects. Nano Lett. 2006; 6:669–76. [PubMed: 16608262]

40. Folkman J. Tumor angiogenesis: therapeutic implications. N Engl J Med. 1971; 285:1182–6. [PubMed: 4938153]
41. Folkman J. Role of angiogenesis in tumor growth and metastasis. Semin Oncol. 2002; 29(6 Suppl 16):15–8. [PubMed: 12516034]
42. Folkman J. Angiogenesis: an organizing principle for drug discovery? Nat Rev Drug Discov. 2007; 6:273–86. [PubMed: 17396134]
43. Abdollahi A, Griggs DW, Zieher H, Roth A, Lipson KE, Saffrich R, et al. Inhibition of alpha v beta 3 integrin survival signaling enhances antiangiogenic and antitumor effects of radiotherapy. Clin Cancer Res. 2005; 11:6270–9. [PubMed: 16144931]
44. Wang Y, Wang X, Zhang Y, Yang S, Wang J, Zhang X, et al. RGD-modified polymeric micelles as potential carriers for targeted delivery to integrin-overexpressing tumor vasculature and tumor cells. J Drug Target. 2009; 17:459–67. [PubMed: 19527117]
45. Yin J, Li Z, Yang T, Wang J, Zhang X, Zhang Q. Cyclic RGDyK conjugation facilitates intracellular drug delivery of polymeric micelles to integrin-overexpressing tumor cells and neovasculature. J Drug Target. 2011; 19:25–36. [PubMed: 20233083]
46. Cai W, Wu Y, Chen K, Cao Q, Tice DA, Chen X. *In vitro* and *in vivo* characterization of ^{64}Cu-labeled Abegrin, a humanized monoclonal antibody against integrin alpha v beta 3. Cancer Res. 2006; 66:9673–81. [PubMed: 17018625]
47. Xiong XB, Huang Y, Lu WL, Zhang X, Zhang H, Nagai T, et al. Enhanced intracellular delivery and improved antitumor efficacy of doxorubicin by sterically stabilized liposomes modified with a synthetic RGD mimetic. J Control Release. 2005; 107:262–75. [PubMed: 16125816]
48. Cai W, Chen K, Mohamedali KA, Cao Q, Gambhir SS, Rosenblum MG, et al. PET of vascular endothelial growth factor receptor expression. J Nucl Med. 2006; 47:2048–56. [PubMed: 17138749]
49. Hong H, Benink HA, Zhang Y, Yang Y, Uyeda HT, Engle JW, et al. HaloTag: a novel reporter gene for positron emission tomography. Am J Transl Res. 2011; 3:392–403. [PubMed: 21904659]
50. Hong H, Yang Y, Zhang Y, Engle JW, Barnhart TE, Nickles RJ, et al. Positron emission tomography imaging of CD105 expression during tumor angiogenesis. Eur J Nucl Med Mol Imaging. 2011; 38:1335–43. [PubMed: 21373764]
51. Hong H, Severin GW, Yang Y, Engle JW, Zhang Y, Barnhart TE, et al. Positron emission tomography imaging of CD105 expression with ^{89}Zr-Df-TRC105. Eur J Nucl Med Mol Imaging. 2012; 39:138–48. [PubMed: 21909753]
52. Kreutzer G, Ternat C, Nguyen TQ, Plummer CJG, Manson JAE, Castelletto V, et al. Water-soluble, unimolecular containers based on amphiphilic multiarm star block copolymers. Macromolecules. 2006; 39:4507–16.
53. Bae YH, Jang WD, Nishiyama N, Fukushima S, Kataoka K. Multifunctional polymeric micelles with folate-mediated cancer cell targeting and pH-triggered drug releasing properties for active intracellular drug delivery. Mol Biosyst. 2005; 1:242–50. [PubMed: 16880988]
54. Cai W, Chen K, Li ZB, Gambhir SS, Chen X. Dual-function probe for PET and near-infrared fluorescence imaging of tumor vasculature. J Nucl Med. 2007; 48:1862–70. [PubMed: 17942800]
55. Liu Z, Cai W, He L, Nakayama N, Chen K, Sun X, et al. *In vivo* biodistribution and highly efficient tumour targeting of carbon nanotubes in mice. Nat Nanotechnol. 2007; 2:47–52. [PubMed: 18654207]

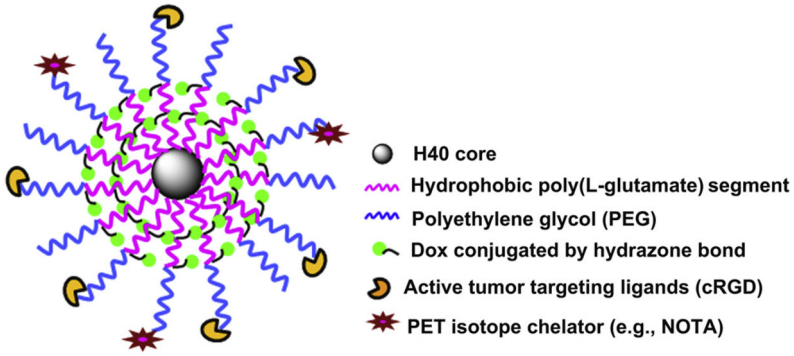

Fig. 1.
A schematic illustration of the multifunctional H40-DOX-cRGD nanocarriers for tumor-targeted drug delivery and PET imaging.

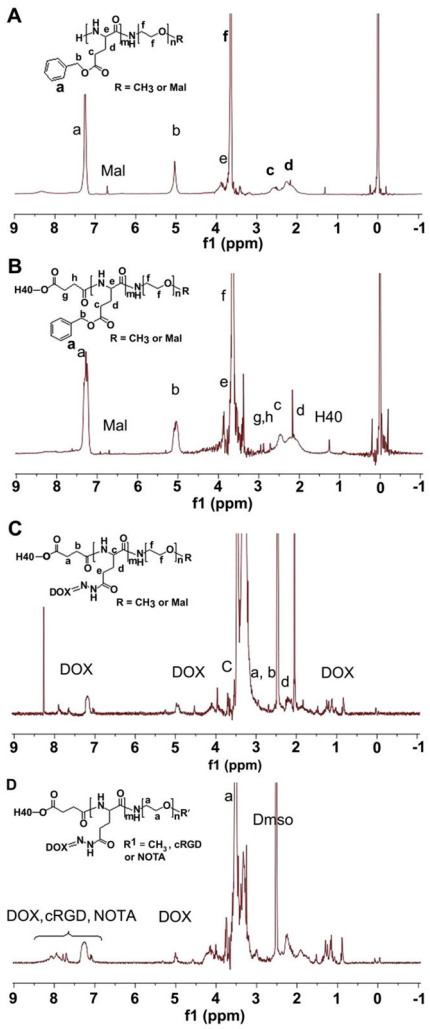

Fig. 2.

^{1}H NMR spectrum of (A) PBLG-*b*-PEG-Mal, (B) H40-PBLG-*b*-PEG-OCH_3/Mal, (C) H40-P(LG-Hyd-DOX)-*b*-PEG-OCH_3/Mal, (D) H40-P(LG-Hyd-DOX)-*b*-PEG-OCH_3/cRGD/NOTA.

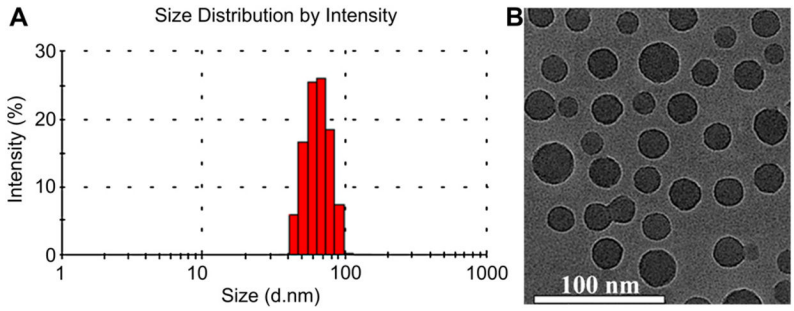

Fig. 3.

The (A) size distribution and (B) morphology of H40-DOX-cRGD nanocarriers as measured by DLS and TEM, respectively.

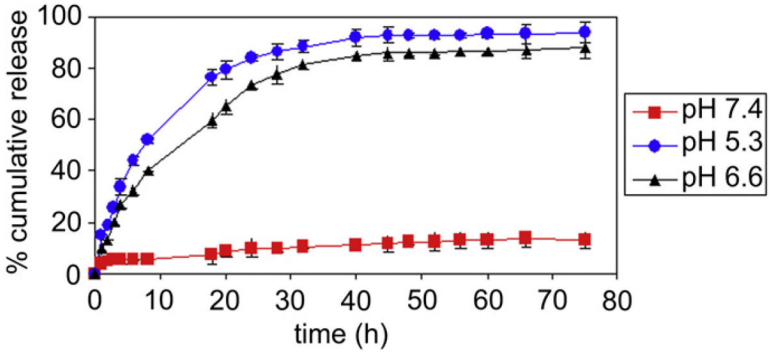

Fig. 4.
In vitro DOX release profiles of H40-DOX-cRGD at a pH value of 5.3, 6.6, and 7.4.

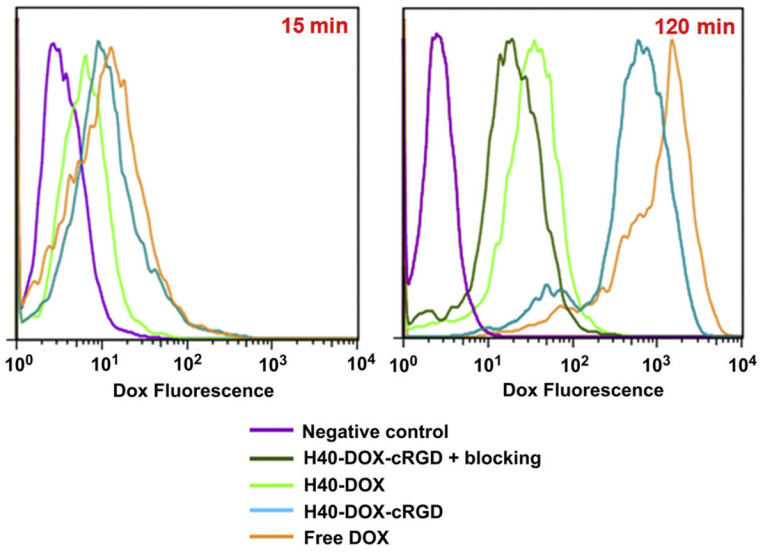

Fig. 5.

Flow cytometry analysis of U87MG human glioblastoma cells treated with free DOX, H40-DOX, H40-DOX-cRGD, or H40-DOX-cRGD with a blocking dose of cRGD (all with equivalent DOX concentration of 20 μg/ml), or medium alone (control) for 15 and 120 min at 37 °C.

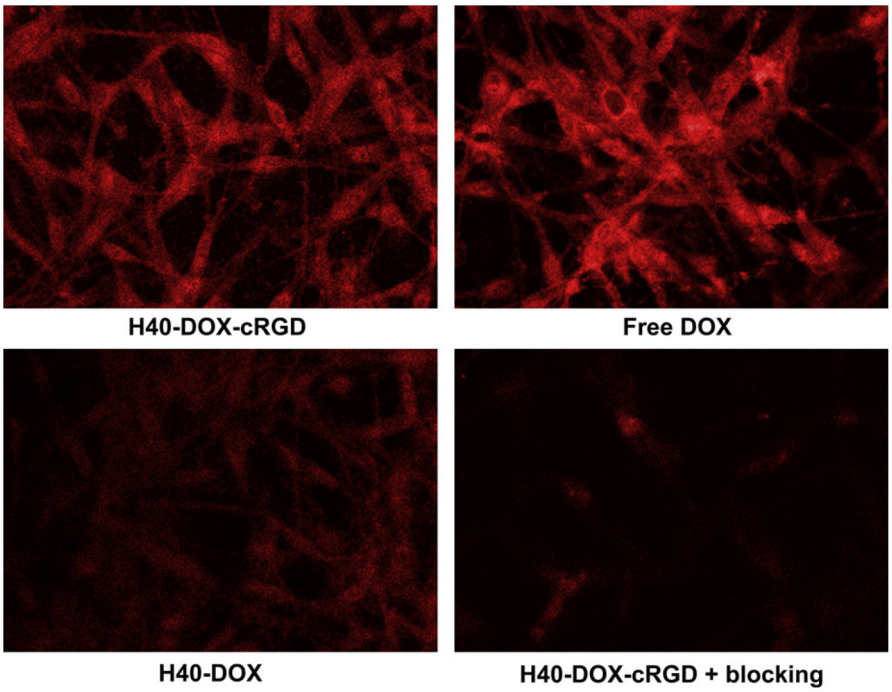

Fig. 6.

Confocal laser scanning microscopy images of U87MG cells incubated with free DOX, H40-DOX, H40-DOX-cRGD, or H40-DOX-cRGD with a blocking dose of cRGD at 37 °C for 2 h. All samples have a DOX concentration of 20 μg/ml.

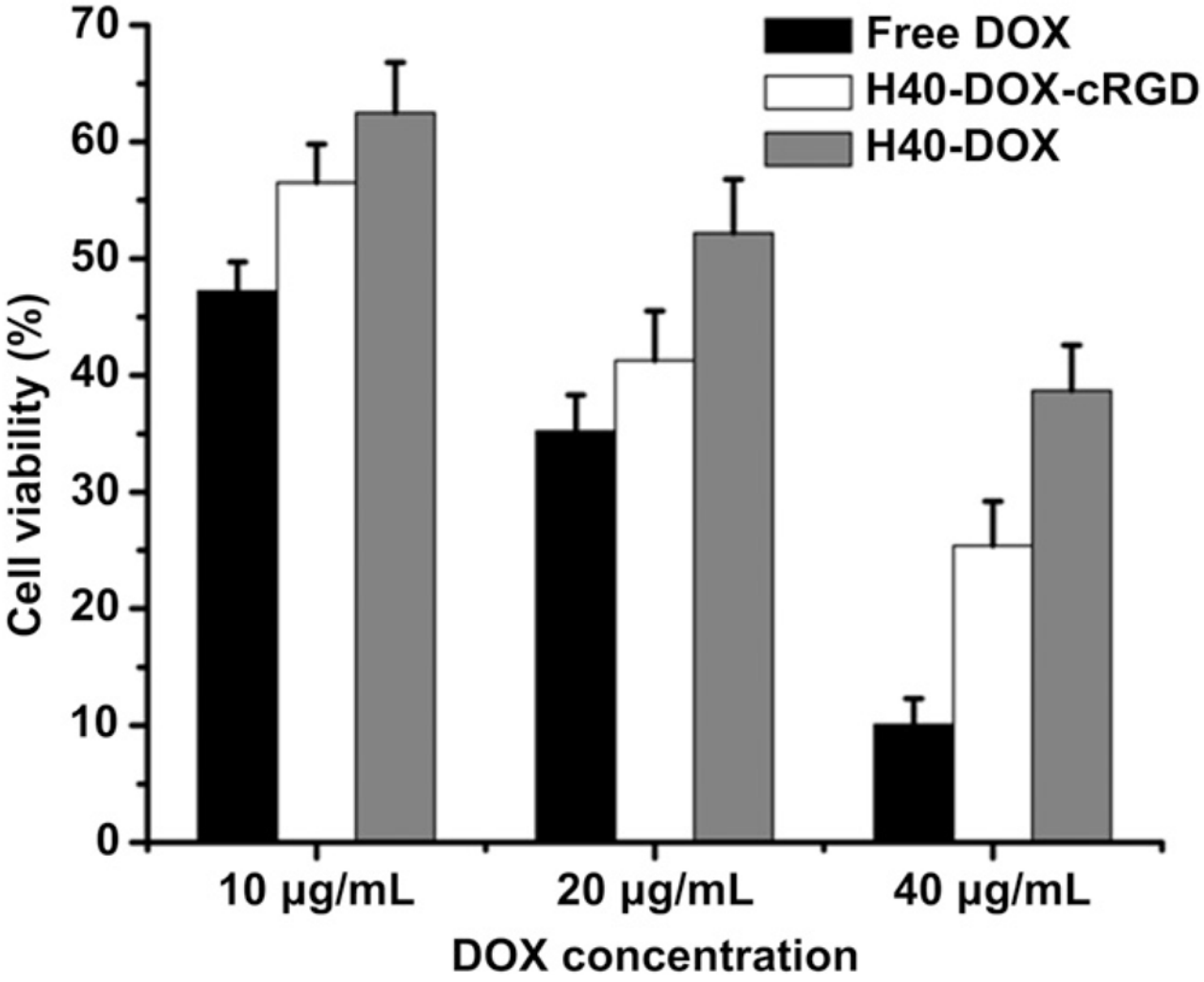

Fig. 7.
Cytotoxicity of free DOX, H40-DOX, or H40-DOX-cRGD to U87MG cells at various DOX concentrations.

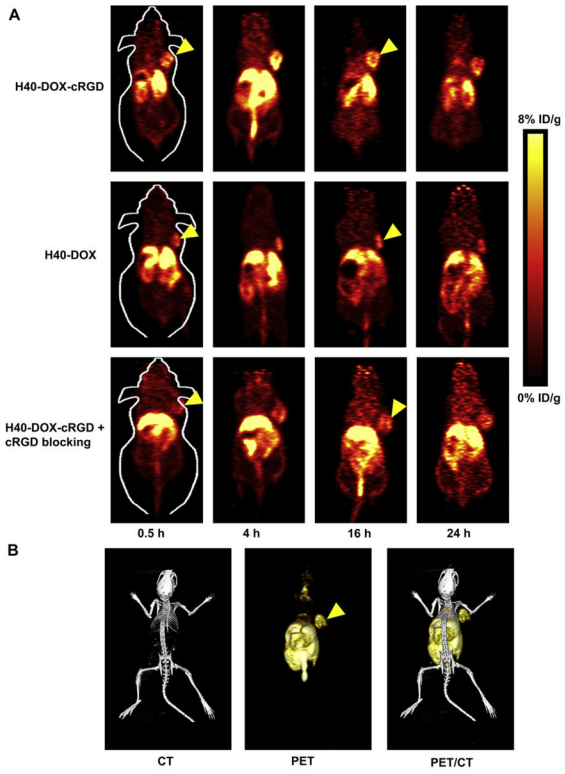

Fig. 8.

Positron emission tomography imaging of ^{64}Cu-labeled nanocarriers in U87MG tumor-bearing mice. (A) Serial coronal PET images of U87MG tumor-bearing mice at various time points post-injection of H40-DOX-^{64}Cu, H40-DOX-cRGD-^{64}Cu, or H40-DOX-cRGD-^{64}Cu with a blocking dose of cRGD. (B) Representative PET/CT images of a U87MG tumor-bearing mouse at 4 h post-injection of H40-DOX-cRGD-^{64}Cu.

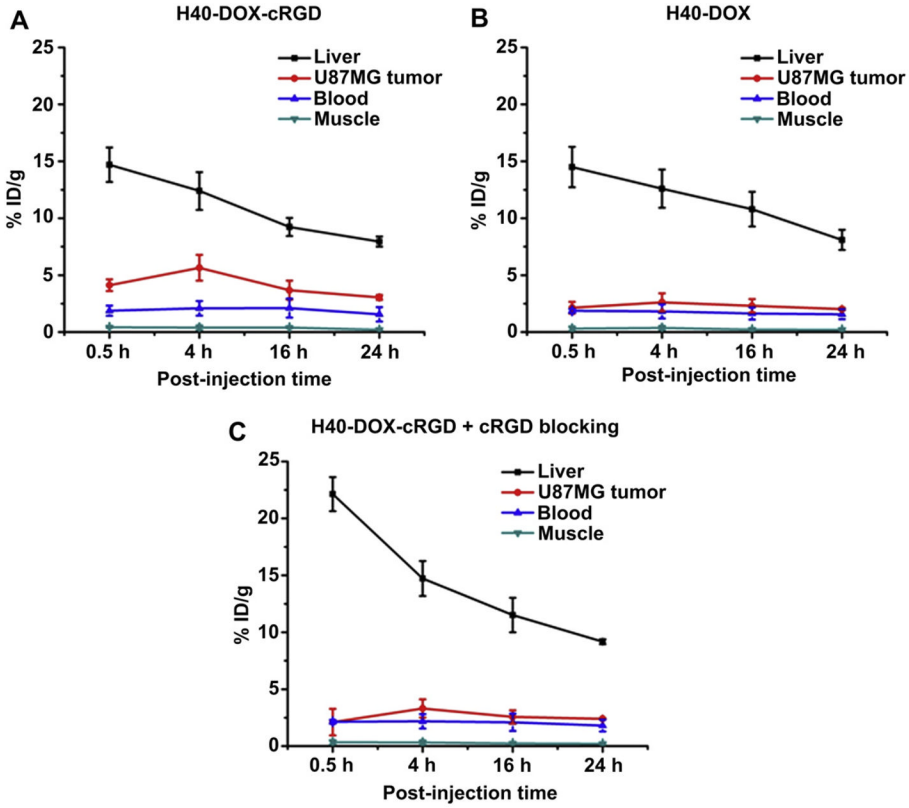

Fig. 9.

Region-of-interest analysis and biodistribution studies. (A) Time-activity curves of the U87MG tumor, liver, blood, and muscle upon intravenous injection of H40-DOX-cRGD-^{64}Cu (n = 3). (B) Time-activity curves of the U87MG tumor, liver, blood, and muscle upon intravenous injection of H40-DOX-^{64}Cu (n = 3). (C) Time-activity curves of the U87MG tumor, liver, blood, and muscle upon intravenous injection of H40-DOX-cRGD-^{64}Cu with a blocking dose of cRGD (n = 3).

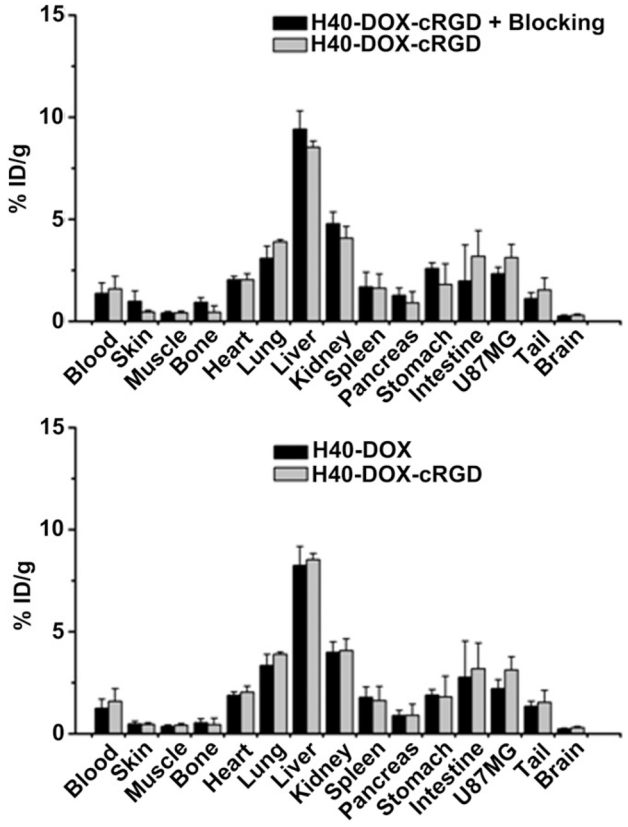

Fig. 10.

Biodistribution of H40-DOX-^{64}Cu, H40-DOX-cRGD-^{64}Cu, and H40-DOX-cRGD-^{64}Cu with a blocking dose of cRGD in U87MG tumor-bearing mice at 24 h post-injection (n = 3).

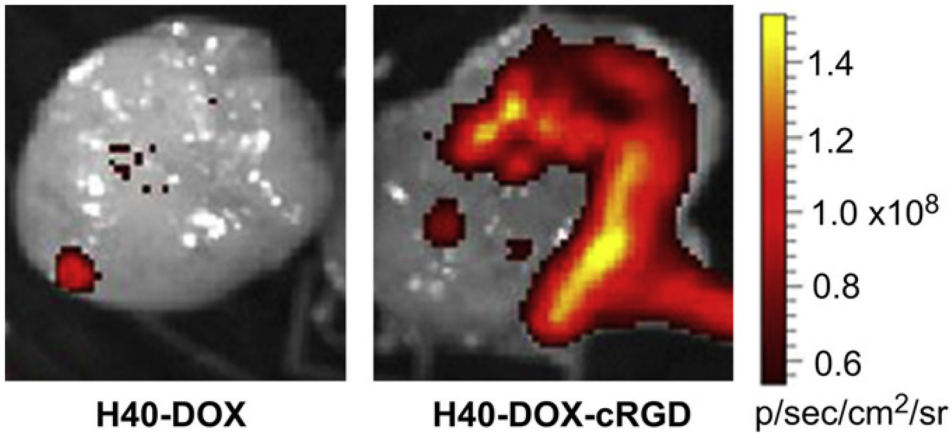

Fig. 11.

Ex vivo fluorescence imaging of a U87MG tumor, with the excitation and emission set for detecting DOX fluorescence, harvested from mice injected with H40-DOX-^{64}Cu or H40-DOX-cRGD-^{64}Cu.

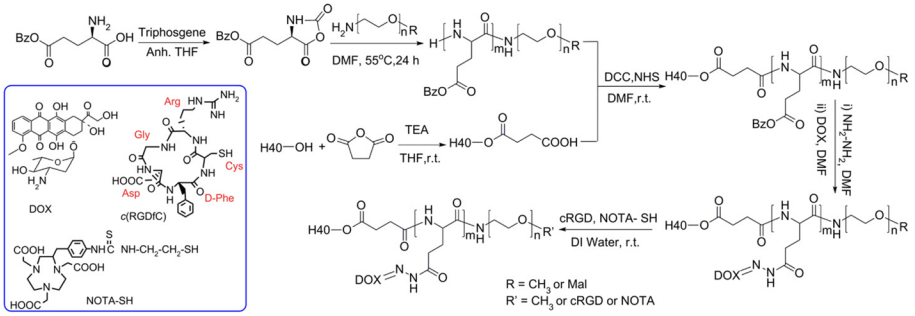

Scheme 1.

The synthetic scheme for the multifunctional H40-DOX-cRGD-^{64}Cu nanocarriers.

Table 1

Molecular weights of H40-COOH, PBLG-*b*-PEG-Mal, PBLG-*b*-PEG-OCH_3 and H40-PBLG-*b*-PEG-OCH_3/Mal.

Sample	M_n	M_w	M_w/M_n
H40-COOH	7577	12502	1.65
PBLG-b-PEG-Mal	7330	8503	1.16
PBLG-b-PEG-OCH_3	6798	8157	1.20
H40-PBLG-b-PEG-OCH_3/Mal	145385	220985	1.52